

10 Dynamical Mean-Field Theory and the Mott Transition

Marcelo Rozenberg

CNRS

Laboratoire de Physique des Solides

Université Paris-Sud, Bât. 510, Orsay 91405, France

Contents

1	Introduction	2
1.1	Strongly correlated systems	2
1.2	Kondo model and Kondo problem	4
2	Dynamical mean-field theory: a primer	6
2.1	Green functions in a nutshell	6
2.2	The DMFT self-consistency equations	8
2.3	DMFT on the Bethe lattice	10
2.4	Quantum impurity problem solvers	13
2.5	Long-range order	15
3	The Mott-Hubbard transition in DMFT	16
3.1	V_2O_3 a strongly correlated material with a metal-insulator transition	17
3.2	The Mott-Hubbard transition	18
3.3	Band-structure evolution across the metal-insulator transition	19
3.4	Coexistence of solutions and the first-order transition line	21
3.5	Endless directions	22
4	Hands-on exercise (with IPT code): the Mott-Hubbard transition	29

1 Introduction

The discovery of the high-temperature cuprate superconductors in the late 80's triggered a strong interest in the physics of transition-metal oxides. It was soon realized that understanding these systems posed a significant theoretical challenge, namely, to describe electronic systems where the independent-electron approximation fails. This became known as the problem of strongly correlated electron systems, and to a large extent remains a challenge. Nevertheless, some significant progress has been accomplished. In this lecture we shall be concerned with a particularly successful approach, namely, dynamical mean-field theory (DMFT), which was developed in the 90's and has allowed to gain new insights into the problem of strong correlations. Specifically, it provided a significant advance in our understanding and description of one of the classic problems in the field, the Mott metal-insulator transition. For a detailed account on how DMFT was developed, the interested reader is referred to the review article [1]. The goal of the present lecture is to introduce DMFT and its application to the problem of the Mott-Hubbard transition in a pedagogical manner, putting emphasis on the new concepts that it brought to light. The lecture is aimed at final-year undergraduates, beginning graduates, or anybody looking for an accessible presentation to the concepts of DMFT, *including experimentalists*. The lecture is supplemented with a computational code, which allows the interested reader to solve the basic DMFT equations. We also propose a set of problems that will guide the reader in the discovery of the physics of the Mott-Hubbard metal-insulator transition.

We shall begin by illustrating, from an experimental point of view, the manifestations of strong correlation phenomena with special attention to that of the Mott transition. We shall then describe in simple terms the DMFT approach by drawing an analogy with the classic mean-field theory of spin models. We then move on to consider the solution of the prototype model of strongly correlated systems, the Hubbard model, which is a minimal model to capture the metal-insulator transition. We shall discuss the transition as a function of interaction strength, temperature, and doping in both, the paramagnetic and the antiferromagnetic phase. We shall describe some basic experimental data on a material that is widely considered to exhibit an actual Mott transition and discuss the connection to theoretical results of the Hubbard model within DMFT.

1.1 Strongly correlated systems

How do we know that we are dealing with a strongly correlated system? This question is important, because the models and their solutions should illustrate precisely those aspects. There are a few physical phenomena which we may consider to be key. The first that we can mention is the presence of complex phase diagrams (Fig. 1). Ordinary materials, are either metals or insulators, or even semiconductors if their gaps are small with respect to room temperature. Common examples are gold, diamond (gap 5.5 eV), and silicon (gap 0.67 eV), respectively. They are relatively easy to understand already by looking whether the outermost electronic orbital shell is partially filled or not. In the case of carbon, the $2p$ orbital has two electrons and this permits different structural arrangements that lift the orbital degeneracy. Thus if the degeneracy is fully

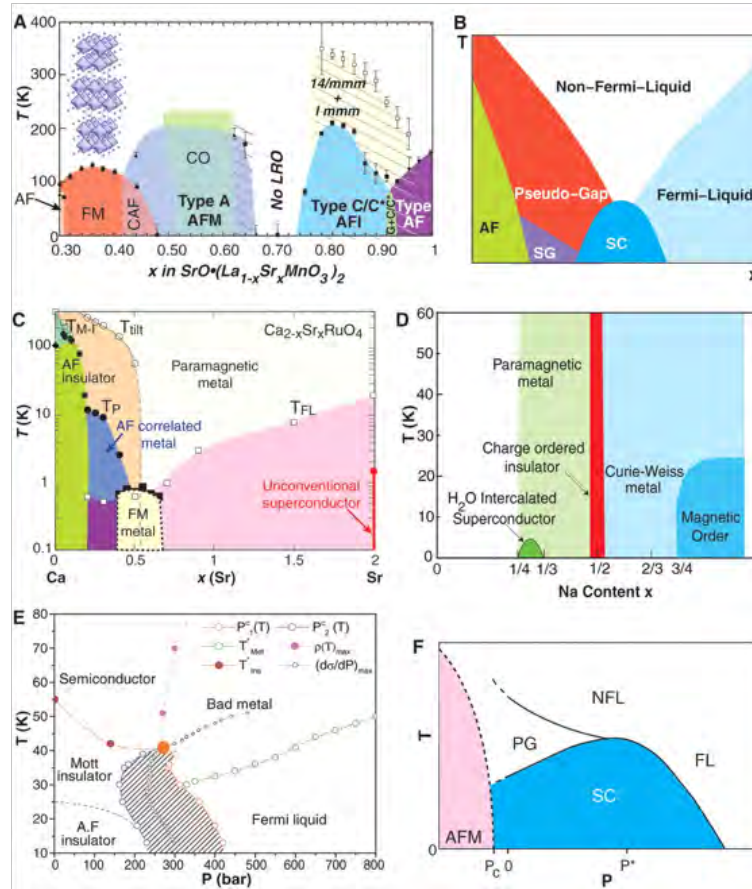


Fig. 1: A complex phase diagram is characteristic of systems with strong electronic correlations. Examples from manganites (A), cuprates (B), ruthenates (C), cobaltates (D), 2-d κ -organics (E), and heavy fermions (F). From [2].

lifted, the $2p$ band is full as in diamond, but if not, it is metallic as in graphite. In the case of gold, the outermost shell is the partially filled $6s^1$, which leads to a metallic structure. These simple materials remain in their stable phase upon heating from low temperatures, without significant changes in their electronic structure. Only at very large temperatures, well above room temperature, the crystalline structure may eventually give up due to phonon excitations. Strongly correlated systems are different. They exhibit dramatic changes in their electronic properties, even at temperatures smaller than room temperature. Examples of these phenomena are the metal insulator transition in V_2O_3 and in the family of nickelates $XNiO_3$ ($X = La, Sm, Pr, \text{etc.}$) the magneto-resistance of manganites $La_{1-y}X_yMnO_3$ ($X = Sr, Ca, \text{etc.}$) and the superconductivity in cuprates such as $La_{2-y}Sr_yCuO_4$, $Bi_2Sr_2Ca_1Cu_2O_{8+y}$, $YBa_2Cu_3O_{7-y}$, $HgBa_2Ca_2Cu_3O_8$, among many others [2]. Iridates, such as Sr_2IrO_4 [3, 4] are currently receiving a great deal of attention for their potential “topological” properties. And we may also mention more exotic structures, such as the molecular crystals of “buckyballs” A_3C_{60} ($A = K, Rb, Cs, \text{etc.}$) that may exhibit superconductivity at $\sim 35K$ [5, 6]. These changes in their electronic transport properties are also correlated with anomalous spectroscopic properties, which involve transfer of spectral intensity that takes place over energy scales of the order of an eV. This becomes significant when we realize that $1 \text{ eV} \sim 11000 \text{ K}$. So the question is how, by heating up a material to $\sim 100 \text{ K}$, we may observe changes on energy scales 100 times larger.

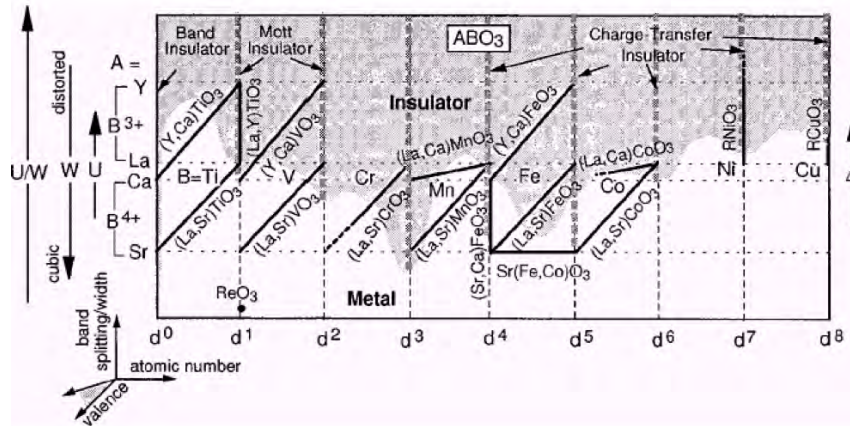


Fig. 2: Schematic phase diagram of transition-metal oxides as a function of the partial filling of the 3d-orbital band and the intensity of Coulomb correlations. Mott insulators are found at integer fillings of the d-shell. From [7].

The most amusing playground for strongly correlated physics, from the point of view of materials, has been that of transition-metal oxides. In particular those transition metals that occupy the third row of the periodic table, filling the 3d orbital shell. As a function of the filling we find a large variety of oxide materials, which are expected to be metals from density-functional theory (DFT) calculations, but are found to be insulators, as illustrated in the Fig. 2. Moreover, those unexpected insulators lead to anomalous metallic states upon chemical doping. A survey of those systems has been condensed into an excellent review by Imada, Fujimori, and Tokura [8]. A practical, but certainly non-rigorous definition of strongly correlated systems could be given: They are those materials whose electronic state and band-structure fail to be described by DFT.

1.2 Kondo model and Kondo problem

One of the oldest problems in strongly correlated materials, and certainly one of the, conceptually, most important, is that of the observed minimum of the resistivity in metals with magnetic impurities, which led to the formulation of the Kondo model. The physical phenomenon consists on the observation of a minimum in the resistivity of an ordinary metal with a small amount of magnetic impurities, such as gold with Mn impurities, as schematically depicted in Fig. 3. The problem was theoretically addressed by Kondo, who considered a Hamiltonian of an ordinary metal of bandwidth W , interacting with an embedded single magnetic impurity with a spin interaction J . Kondo showed that diagrammatic perturbation theory broke down at a low temperature, where logarithmic divergences developed. This became the Kondo problem, which led to very important developments. We may mention a wonderful paper by Anderson, known as “Poor’s man scaling,” which was an important step in the right direction. Eventually, Wilson invented the numerical renormalization group (NRG) in the 70’s, providing an exact numerical solution and a conceptual breakthrough. The problem was analytically solved by Andrei and Tselvik in the 80’s using the Bethe Ansatz, a highly technical mathematical methodology. An important concept that emerged from the solution of the Kondo problem was that of the

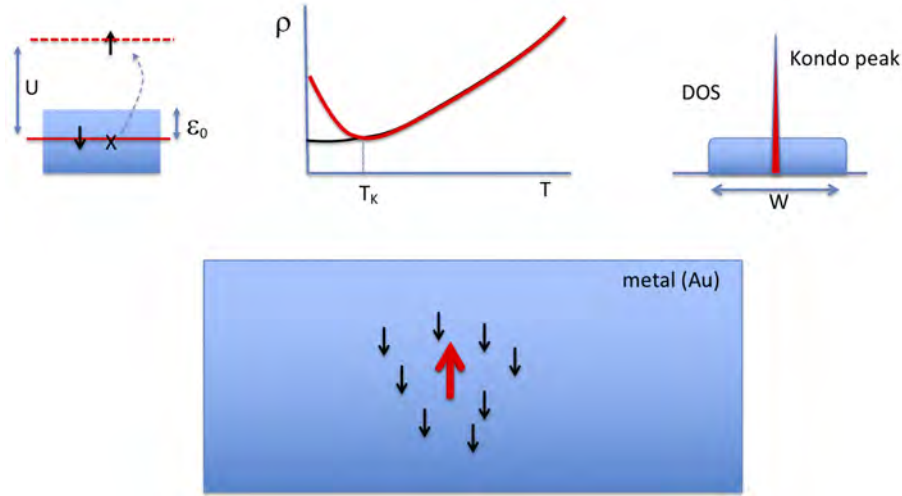


Fig. 3: Schematic illustration of the Kondo effect. Top: (left) The magnetic moment of an impurity site emerges when the second electron is hindered to doubly-occupy a site below the Fermi sea due to the interaction energy cost U (dotted energy level). The physical manifestation of the Kondo effect are: (middle) a logarithmic increase of the resistivity at low T (red line), with respect to the non-magnetic impurity scattering (black line); and (right) a sharp resonance in the DOS at the Fermi energy (the Kondo peak). Bottom: Illustration of the (dynamic) screening of the magnetic impurity by the conduction electrons forming a many-body singlet state.

Kondo resonance and the Kondo temperature. The former is a peak in the local density of states (at the site of the magnetic impurity), which corresponds to a many-body state where the metallic electrons dynamically screen the magnetic moment of the impurity, forming a singlet state. This phenomenon occurs below the Kondo temperature, which is exponentially small: $T_K \sim W e^{-W/J}$. The solution of this problem already illustrates the characteristics of strong correlations we have mentioned before: There is a change in the electronic conduction (Kondo minimum) and in the spectral properties (Kondo resonance), which all occur at a low temperature (Kondo temperature) well below the bare energies scales of the model (W and $J \sim \text{eV}$, while $T_K \sim 10 \text{ K}$).

The Kondo model can be generalized into the single impurity Anderson model (SIAM), where the magnetic impurity is represented by an atomic site with energy $\varepsilon_0 \leq 0$ (beneath the surface of the Fermi sea) and a local Coulomb repulsion U . For large values of U , the double occupation of the site is penalized so the orbital occupied by only one electron describes a magnetic impurity. The atomic site is hybridized with the conduction band of the metallic host via an amplitude V . This permits the conduction electrons to briefly (doubly) occupy the impurity site, screening its spin. Because of the high energetic cost U , one of the electrons of the impurity returns to the metal, which may produce a “spin-flip” of the impurity spin. These processes lead to the formation of a non-magnetic many-body state involving both the impurity and the conduction electron degrees of freedom. Similarly as in the Kondo model, this occurs below a low temperature scale. The relation between the two models is $J \sim V^2/U$, for the case where $\varepsilon_0 = 0$ and U is large. An instructive problem to solve is to consider a minimal SIAM as a two-site Hamiltonian problem, where one “impurity” site has energy ε_0 and a correlation term

$Un_{0\uparrow}n_{0\downarrow}$, the other “conduction band” site has energy zero, and they are hybridized by a hopping amplitude V . The density of states (DOS) of the sites can be computed, along with all interesting observables, such as the magnetic correlation functions and the magnetic moments, with relatively small numerical effort, even at finite T . Already the DOS will show a striking temperature dependence, with transfers of spectral weight across large energy scales, the emergence of a precursor of the Kondo peak, and the magnetic screening of the impurity spin. As we shall see below, the importance of the Kondo and the SIAM is not only conceptual: they form the very heart of the DMFT method.

2 Dynamical mean-field theory: a primer

The best way to introduce dynamical mean-field Theory (DMFT) is to draw an analogy with the familiar mean-field theory of the Ising model, which is a text book case of statistical physics. However, before doing that we need to give a brief introduction to Green functions (GF), since these mathematical objects are central to the formulation of DMFT. Unlike the Ising spins, GF are frequency (or time) dependent objects, hence the “dynamical” aspect of the DMFT. We shall avoid mathematical rigor and focus just on the aspects of the GF that we need to carry on the discussion. We shall avoid using vectors, also in the sake of keeping the notation light. The meaning should be always clear from the context. There are excellent text books on the topic of GFs, a classic one is that by G. Mahan [9].

2.1 Green functions in a nutshell

Physically, the GF are mathematical objects that characterize the propagation of particles through the lattice. Therefore they have site and time coordinates, or equivalently, lattice momentum and frequency (k, ω) . In this case, the physical interpretation is that the GF describes the process of adding (removing) a particle with energy $\omega > 0$ ($\omega < 0$) and momentum k . The GF are complex functions that are defined on the whole complex plane $G(k, z)$, with $z \in \mathbb{C}$, where $\omega = \text{Re}(z)$. They are analytic, so they are defined on both, the real and imaginary axis. In practice we use both. The real frequency axis GF provide functions that can be compared with experiments. For instance, the imaginary part of the local GF (i.e., at position $x=0$) as a function of real frequency ω is the density of states (DOS) $\rho(\omega)$, which is measured by photoemission and scanning tunneling spectroscopy experiments,

$$\rho(\omega) = -\frac{1}{\pi} \text{Im} G_{\text{loc}}(\omega) = -\frac{1}{\pi} \text{Im} \sum_k G(k, \omega). \quad (1)$$

In contrast to the continuous variable ω , on the imaginary frequency axis the GF is defined on a set of discrete frequencies, called (fermionic) Matsubara frequencies $\omega_n = (2n+1)\pi/\beta$, with $n \in \mathbb{Z}$ and $\beta \equiv 1/T$ is the inverse temperature. The interest of using GFs on the imaginary axis is that they are often easier to compute than their real axis counterparts. There is an important

price to pay, however, which is the need to analytically continue the $G(k, i\omega_n)$ to obtain the $G(k, \omega)$ so comparisons can be made with experiments.

The simplest GF is that of a single orbital state, isolated, and of energy ε_0 ,

$$G(\omega) = \frac{1}{\omega + \varepsilon_0 - i\eta}. \quad (2)$$

The imaginary part (i.e., the DOS) has a delta function from the simple pole at ε_0 . For a tight binding Hamiltonian, with a band that disperses as ε_k , the GF becomes a function of k and ω

$$G(k, \omega) = \frac{1}{\omega - \varepsilon_k + i\eta}, \quad (3)$$

whose imaginary part has delta-peaks at the poles of $G(k, \omega)$ that provide the electronic band energy dispersion ε_k , while $i\eta$ provides a small width to the peaks. It is called the *spectral function*, $A(k, \omega) = -\text{Im} G(k, \omega)/\pi$ and is, in principle, measured in ARPES experiments.

The lifetime of the excitations is given by the inverse of the frequency-width of the peaks appearing in the spectral functions $A(k, \omega)$. In a non-interacting system, as in a tight binding Hamiltonian with dispersion ε_k , the single particle states are eigenstates and are stationary, so they have an infinite lifetime. Accordingly, the poles of the GF become infinitely narrow delta-peaks $\delta(k - k_0, \omega - \varepsilon_{k_0})$ in the spectral function.

Interactions, such as on-site Coulomb repulsion, that in the Hubbard model have the same form, $U n_{\uparrow} n_{\downarrow}$, as in the SIAM affect the non-interacting band structure. They may change the energy dispersion and can also change the lifetime of the excitations. In extreme cases, they can qualitatively change the energy dispersion or “electronic structure.” We shall see a concrete instance in the Mott-Hubbard metal-insulator transition. Mathematically, the effects of the interactions is encoded in the calculation of another complex function that shares the same analytic properties as the GF. It is called the self-energy $\Sigma(k, \omega)$. Thus solving the many-body problem of an interacting model amounts to obtaining the self-energy. Let’s write down the definitions for the concrete case of a Hubbard model (HM)

$$H = H_0 + U \sum_i n_{i\uparrow} n_{i\downarrow} \quad \text{with} \quad H_0 = -t \sum_{\langle i,j \rangle \sigma} c_{i\sigma}^{\dagger} c_{j\sigma}, \quad (4)$$

where $\langle i, j \rangle$ denote nearest neighbors sites and $n_{i\sigma} = c_{i\sigma}^{\dagger} c_{i\sigma}$. Thus, we have for the GF

$$G_0(k, \omega) = \frac{1}{\omega - \varepsilon_k + i\eta} \quad \text{and} \quad G(k, \omega) = \frac{1}{\omega - \varepsilon_k - \Sigma(k, \omega)}, \quad (5)$$

where G_0 is called the non-interacting GF. We see in the expression of the GF how the Σ function can modify the electronic dispersion of H_0 : $\text{Re} \Sigma$ changes the energy of the excitations, while $\text{Im} \Sigma$ changes their lifetime $\tau_L = 1/\text{Im} \Sigma(\omega=0)$.

Two more definitions will be useful. The notion of quasiparticle residue Z and renormalized mass m^* . They both serve to parametrize the effect of interactions for the low energy band-structure. We can write it as the sum of two contributions

$$G(k, \omega) \approx \frac{Z}{\omega - Z \varepsilon_k} + (1 - Z) G_{\text{inc}}(k, \omega). \quad (6)$$

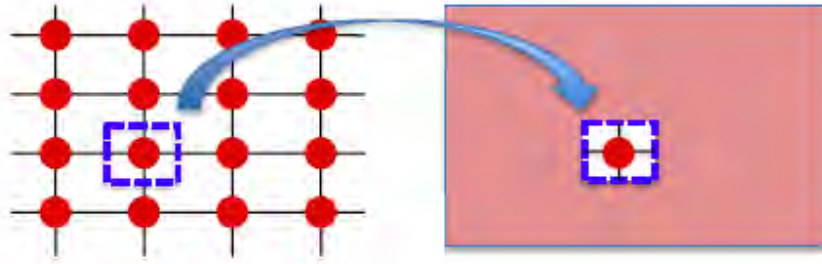


Fig. 4: One site from the lattice is embedded into an effective electronic bath. The bath is self-consistently determined to best represent the lattice environment of the site. This single-site quantum-impurity problem remains a non-trivial many-body problem.

The quasiparticle residue is $0 \leq Z \leq 1$, and represents the part of the DOS which remains with a well defined energy dispersive structure. The excitations are modified as $Z\varepsilon_k$, which implies that the electronic band becomes flatter, i.e., has a higher mass. If $\varepsilon_k = -t \cos(ka) \approx k^2/2m$, we see that $Z\varepsilon_k$ gives an enhanced effective mass $m^* = m/Z > m$. Since the DOS is normalized to 1, the spectral weight which is not in the quasiparticle part at low energy has to appear at a higher energy. This contribution does not have a very well defined dispersion (due to short lifetimes from a large $\text{Im } \Sigma$) and thus we have the factor $1-Z$ in front of the second contribution, which we call *incoherent* G_{inc} .

We have gone fast on these definitions. There are excellent text books for the interested reader to learn more details [9].

2.2 The DMFT self-consistency equations

We use the functional integral formalism to introduce the main DMFT equations. Again, there are excellent text books on that formalism too [10]. The method is based on writing down the action of a Hamiltonian model. We shall skip all the details of the formalism and simply write down directly the most important expressions, which should be clear enough. For simplicity we shall focus on the Hubbard model (HM) defined above in Eq. (4). The action of the HM reads

$$S = \int_0^\beta d\tau \left(\sum_{i\sigma} c_{i\sigma}^\dagger \partial_\tau c_{i\sigma} - t \sum_{\langle i,j \rangle \sigma} c_{i\sigma}^\dagger c_{j\sigma} - \mu \sum_{i\sigma} n_{i\sigma} + U \sum_i n_{i\uparrow} n_{i\downarrow} \right). \quad (7)$$

The model is defined on a given lattice. The next step is, as in standard mean-field theory, to single out a site and try to replace the original lattice problem by an effective *quantum impurity problem* (QIP) embedded in a medium that is determined so to best represent the original environment of the site. This is pictorially represented in Fig. 4. More concretely, we split the action into that of the single lattice site $i = 0$ at the “origin,” S_0 , the rest of the lattice, $S^{(0)}$, and the coupling between them, ΔS : $S = S_0 + \Delta S + S^{(0)}$

$$S_0 = \int_0^\beta d\tau \left(c_{0\sigma}^\dagger (\partial_\tau - \mu) c_{0\sigma} + U n_{0\uparrow} n_{0\downarrow} \right) \quad \text{and} \quad \Delta S = \int_0^\beta d\tau \left(-t \sum_{\langle i,0 \rangle \sigma} c_{i\sigma}^\dagger c_{0\sigma} + c_{0\sigma}^\dagger c_{i\sigma} \right). \quad (8)$$

By means of standard field-theory methods we integrate out the rest of the lattice and write the full effective action on the lattice site at the origin alone as

$$S_{\text{eff}} = \int_0^\beta d\tau \left(c_{0\sigma}^\dagger (\partial_\tau - \mu) c_{0\sigma} - \sum_{ij\sigma} t_{0i} t_{j0} G_{ij}^{(0)} + \dots + U \sum_i n_{i\uparrow} n_{i\downarrow} \right). \quad (9)$$

$G_{ij}^{(0)}$ denotes the exact propagator of the lattice with the 0-site excluded and (...) stand for higher order terms in the hopping t . Up to now there are no approximations, but the problem remains too hard to deal with. DMFT corresponds to taking the limit of large dimensionality, large lattice connectivity or large lattice coordination. An evident problem is that the number of neighbor sites to 0 grows to infinity (i.e., the band-width would grow to ∞). Metzner and Vollhardt [11] realized that the reasonable way to cure this problem is by rescaling the hopping amplitude $t \rightarrow t/\sqrt{d}$, where d is the number of spatial dimensions. The simplest way to see this is noting that the typical value of the kinetic energy for a random k vector is $E_{\text{kin}} = \sum_i^d -t \cos(ka) \propto (\sqrt{d}t)^2$ (using the central limit theorem). A key consequence of this scaling is that the (...) in Eq. (9) vanish (as they are higher order in t), which is a great simplification. Thus, we recognize from S_{eff} the quantum impurity problem that we were looking for

$$S_{\text{QIP}} = \sum_{n\sigma} c_{0\sigma}^\dagger \mathcal{G}_0^{-1}(i\omega_n) c_{0\sigma} + \beta U n_{0\uparrow} n_{0\downarrow}, \quad (10)$$

with the “non-interacting” GF of the QIP defined as

$$\mathcal{G}_0^{-1} = i\omega_n + \mu - t^2 \sum_{(ij)} G_{ij}^{(0)}(i\omega_n), \quad (11)$$

where (ij) denotes the sites neighboring 0 and we went from imaginary time τ to the Matsubara frequency ω_n representation. Notice that the \mathcal{G}_0 is the bare propagator of the QIP and should not be confused with G_0 , which is the bare local propagator of the lattice. The last term represents the environment of the impurity, which still needs to be determined. Its physical interpretation is that an electron at the impurity site has an amplitude t to hop out to a neighbor site i , then it propagates through the rest of the lattice from i to j with $G_{ij}^{(0)}$, and returns from site j back to the impurity site with a second hop t . The 0 index in \mathcal{G}_0 indicates that it is the non-interacting GF of the impurity problem, but this object is, in general, different from the original lattice local non-interacting GF.

$G_{ij}^{(0)}$ is a fully interacting GF whose solution is, in principle, at least as hard as the original problem. So we need to do something about it. Diagrammatically, we can write the cavity GF

$$G_{ij}^{(0)} = G_{ij} - \frac{G_{i0} G_{0j}}{G_{00}}, \quad (12)$$

where the second term subtracts from the first all the diagrams that go back to the origin, and its denominator takes care of the double counting of local diagrams. Notice that $G^{(0)}$ has now been written in terms of the lattice GF. If we *assume* a k -independent self-energy we can express the lattice GF in real space by summing over specifying the geometry of the lattice and Fourier

transforming. Then, inserting Eq. (12) into (11) the sum over spatial indices can be performed and one obtains the self-consistency equation [1]

$$\mathcal{G}_0^{-1}(i\omega_n) - \Sigma(i\omega_n) = \sum_k \frac{1}{i\omega_n + \mu - \varepsilon_k - \Sigma(i\omega_n)} = G_{\text{loc}}(i\omega_n). \quad (13)$$

This expression is valid for all lattices. For instance, on a hyper-cubic lattice, which is the generalization of the square and cubic lattices to high dimensions, the integral over k can be done as a sum over the hyper-cubic lattice single-particle energies ε

$$G_{\text{loc}}(i\omega) = \int_{-\infty}^{+\infty} \frac{1}{i\omega_n + \mu - \varepsilon - \Sigma(i\omega_n)} \text{DOS}(\varepsilon) d\varepsilon, \quad (14)$$

where

$$\text{DOS}(\varepsilon) = \frac{e^{-\varepsilon^2/2t^2}}{t\sqrt{2\pi}} \quad (15)$$

is a Gaussian function (again using the central limit theorem).

A few comments are in order now. From Eq. (13) and (10) we see that $\Sigma(i\omega_n)$ is the self-energy of the QIP. It is obtained as the solution of the many-body single-site problem, i.e., the QIP, which depends on \mathcal{G}_0 . Thus, we can write $\Sigma = \Sigma[\mathcal{G}_0]$ so that the self-consistent nature of Eq. (13) becomes evident. The key feature that links this equation to the original lattice problem is that it can be shown that *at the self-consistent point*, the QIP self-energy $\Sigma(i\omega_n)$ *coincides* with the exact self-energy of the lattice $\Sigma(i\omega_n)$ [1]. Crucially, in the limit of large dimensionality or lattice connectivity and with the re-scaling of the hopping made above, the lattice self-energy is k -independent, which validates the assumption made to obtain Eq.13 [1]. Hence, at the self-consistent point, we also recognize on the right hand side of Eq. (13) the *local* GF of the lattice problem $G_{\text{loc}}(i\omega_n)$, which we set out to solve.

So the issue is now reduced to obtaining the self-energy, given the impurity \mathcal{G}_0 . We see that given a guess for \mathcal{G}_0 , we solve the many-body QIP to obtain a guess for Σ . We input that into the r.h.s. of Eq. (13) to obtain a guess for G_{loc} . Then, from $G_{\text{loc}} + \Sigma$ we get a *new* guess for \mathcal{G}_0 . This has to be iterated until self-consistency is attained. Then the problem is solved as we obtain the DMFT solution for the *lattice* GF as

$$G(k, i\omega_n) = \frac{1}{i\omega_n - \varepsilon_k - \Sigma(i\omega_n)}. \quad (16)$$

This equation, with a k -independent Σ is exact for lattices in infinite spatial dimensions or infinite connectivity. However, the procedure may be adopted for lattices in any dimension and that case the DMFT and the k -independence of Σ become an approximation, which is at the root of the realistic DMFT approach for materials that we shall describe later.

2.3 DMFT on the Bethe lattice

Another illuminating light can be cast on the DMFT self-consistency condition by considering the Bethe lattice. There are two main features that make this lattice a very popular choice for

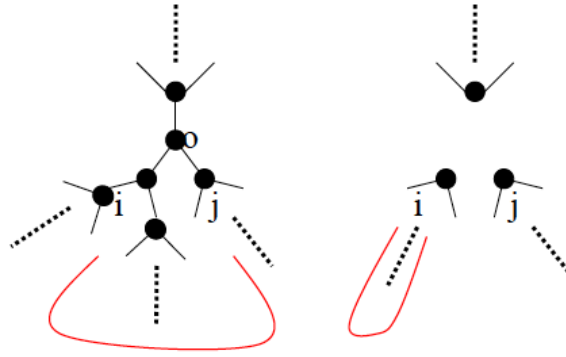


Fig. 5: The Bethe lattice (for connectivity $d = 3$). The red line indicates the “cavity” propagator. When the origin (0) is taken out, the electrons have to leave and return to the origin via the same neighbor site (i), rendering the cavity propagator site-diagonal, cf. Eq. (12).

DMFT studies. The first one is that the DOS(ω) is a semi-circle, which has a finite band-width and band-edges similar to 3D cubic lattices. The second is that the self-consistency equations are easier to derive. The Bethe lattice of coordination z is a “branching tree”, where from each node emanates a number z of branches. In Fig. 13 we show the case $z=3$. In this type of lattice the cavity $G_{ij}^{(0)}$ is easy to obtain. In the left panel of the figure we depict with a red line a propagation from site i to j , both nearest neighbors of the 0-site. The cavity propagator has to be obtained with the 0-site removed. The right panel shows that when we do that, an electron that has hopped from 0 to i can only return back to 0 hopping from i . In other words, $G_{ij}^{(0)} = G_{ii}^{(0)} \delta_{ij}$. Now, if we consider the limit of large lattice coordination, $z \rightarrow \infty$, we see from the right panel of Fig. 5 that the $G_{ii}^{(0)}$ is identical to G_{ii} , which by definition is G_{loc} . Thus, from the cavity Eq. (12)

$$G_{ij}^{(0)} = G_{ii}^{(0)} \delta_{ij} = G_{ii} \delta_{ij} = G_{\text{loc}} \delta_{ij}. \quad (17)$$

Replacing into Eq. (11), we can perform the sum to get

$$\mathcal{G}_0^{-1} = i\omega_n + \mu - t^2 G_{\text{loc}}(i\omega_n), \quad (18)$$

where we used that the hopping is rescaled, as mentioned before, by $t \rightarrow t/\sqrt{z}$. The self-consistency equation for the Bethe lattice has a very compact and intuitive form, and avoids the need of the ε integral of the hyper-cubic case.

From the point of view of the QIP problem we observe that the quantum impurity is embedded in a medium that is nothing but t^2 times the local GF. The problem is dealt with similarly as before: given a guess for the \mathcal{G}_0 , the many-body problem of the 0-site is solved. An interacting GF for the impurity is obtained and a new guess for \mathcal{G}_0 is simply computed from Eq. (18). The iteration proceeds until convergence is attained and at that point, as before, the $G_{\text{loc}}(i\omega_n)$ becomes the local GF of the original lattice problem.

To show that the self-consistency condition obeys the general form of Eq. (13), we first compute the local *non-interacting* Bethe lattice DOS(ε). Since $U=0$, we have $G_{\text{loc}}=\mathcal{G}_0$. Thus, replacing into Eq. (18) and solving the quadratic equation, we can get the $G_{\text{loc}}(i\omega_n)$ and from the

imaginary part of the analytic continuation to the real-frequency axis

$$\text{DOS}(\varepsilon) = \frac{2}{\pi D^2} \sqrt{1 - \left(\frac{\varepsilon}{D}\right)^2} \quad \text{for } |\varepsilon| < D, \quad (19)$$

where we introduced the half-bandwidth $D = 2t$. Inserting this $\text{DOS}(\varepsilon)$ into the general Eq. (14) and using the Dyson equation for the quantum impurity, $G_{\text{loc}}^{-1} = \mathcal{G}_0^{-1} - \Sigma$, one re-derives the Bethe lattice self-consistency condition Eq. (18).

Experience has shown that for simple model Hamiltonians there are no qualitative differences in the DMFT solutions of different lattices, therefore, the simplicity of the Bethe lattice often justifies the choice.

An important feature of the solution is that the lattice self-energy Σ , which coincides with that of the QIP at self-consistency, does not depend on momentum. This is evidently not a characteristic of a Σ in general, so we may ask if this makes sense. Or, in other words, when should we expect Σ to be independent, or weakly dependent, of the momentum? The answer is for physical problems where the stronger interactions are local and when the lattice coordination is large. In fact, the latter follows from a mathematical statement, which is that the DMFT solution becomes exact in the limit of large spatial dimensions [11, 1]. In practice, one may then expect that for cubic, bcc, and fcc lattices with coordinations 6, 8, and $12 \gg 1$, the approach should be reliable. On the other hand, in regard to locality of interactions, we may expect them to dominate the physics when the orbitals are small with respect to the interatomic distances of the material (or more simply to the lattice spacing). This is the case for two types of materials, such as the $3d$ transition-metal oxides and the heavy fermions. Among the first we have the strongly correlated materials that we listed in the Introduction (Sec. 1). Heavy fermions are typically inter-metallic compounds, such as CeCu_6 , CeAl_3 , UBe_{13} , and UPt_3 , that have an ordinary metal and one with active f -electrons, such as the actinides.

How about the case for a material that has a relatively low coordination but does have strong local interactions? That is the case of an important class of materials, the high- T_c cuprate and the iron-based superconductors. Both these systems have layered structures. The answer may depend on the person that this question is asked to. But more fairly, one should say that the relevance of DMFT may depend on the type of physical question that one is asking. We shall see some examples later on that shall illustrate this point.

We can summarize the DMFT method and its self-consistent nature by drawing an analogy with the familiar mean-field theory of an Ising model. This is schematically shown in Fig. 6. On the left panel we have the main DMFT ingredients: a lattice model and Hamiltonian; the mapping to the quantum impurity problem and the effective action of the single-site of the lattice; the restoration of the spatial translation invariance of the lattice by enforcing a self-consistency constraint; and the requirement for a rescaling of the original hopping parameter so that all terms in the model remain of finite energy when one takes the limit of high dimensionality. As we can see in the right panel of the figure, all those ingredients have a counterpart in the Ising model MFT. One can observe that in the latter the local magnetization m (or h_{eff}) is an a priori unknown that needs to be determined, similarly as the \mathcal{G}_0 . Another feature is that the



$$H = - \sum_{i,j,\sigma} t_{ij} c_{i\sigma}^\dagger c_{j\sigma} + U \sum_i n_{i\uparrow} n_{i\downarrow}$$

$$H = \sum_{i,j} J_{ij} S_i S_j$$

$$S_{\text{eff}}[\mathcal{G}_0] = - \iint d\tau d\tau' c_{0\sigma}^\dagger \underline{\mathcal{G}_0^{-1}} c_{0\sigma} + U \int d\tau n_{0\uparrow} n_{0\downarrow} \quad H_{\text{eff}} = \left(\sum_i J_{0i} S_i \right) S_0 = z \underline{J m} S_0 = h_{\text{eff}} S_0$$

$$\underline{\mathcal{G}_0^{-1}} = i\omega_n + \mu - t^2 G(i\omega_n)$$

$$\underline{m} = \langle S_0 \rangle = \tanh(\beta z \underline{J m})$$

$$t_{ij} \sim 1/\sqrt{z}$$

$$J_{ij} \sim 1/z$$

Fig. 6: Analogy between Hubbard model DFMT and Ising model MFT. We highlight the similar role of the “origin” site 0 and the a priori unknown “cavity” or “Weiss field” function $\underline{\mathcal{G}_0^{-1}}$ and the mean magnetization \underline{m} . Also, both methods become exact in the limit of large dimensions (or connectivity z) after the required “rescaling” of the hopping in DMFT and the magnetic interaction in the MFT. Notice that in the Hubbard model the super-exchange $J \sim 4t^2/U$ also becomes rescaled by $1/z$.

numerical difficulty to solve the model is dramatically reduced by mapping to a single site. Solving a single Ising-spin is trivial, however, solving the QIP still remains a difficult many-body problem. A variety of techniques have been developed over the years to obtain reliable numerical solutions.

2.4 Quantum impurity problem solvers

An important technical point that we should mention is the practical solution of the QIP, which remains a non-trivial many-body problem [12]. From the start we should say that despite almost 30 years of work, where a variety of methods have been proposed [13], there is no single ideal one. We shall briefly comment on the most important techniques. We recall that the goal is to solve an arbitrary single-impurity Anderson model (SIAM), where the interacting atomic site is hybridized to an environment, or “bath” that is specified by a $\text{DOS}(\omega)$. In the standard SIAM the bath represents a metal, but in the present case the bath is a function that evolves under the iterative procedure. For a Bethe lattice it coincides with the local GF as we discussed above. The main techniques are the following:

Quantum Monte Carlo: This is a finite temperature method that is performed on the imaginary time axis, so it produces solutions to the model on the Matsubara frequency axis. This has the drawback that it requires the additional step of analytic continuation, which presents significant technical problems regarding the reliability and the precision of the spectra. This

can be mitigated improving the accuracy of the MC calculation. It is perhaps the most powerful method. It was originally implemented via a Trotter expansion of the action and a discrete Hubbard-Stratonovich transformation [14, 1]. More recently, a continuous time formulation was developed, based on a statistical sum of diagrams [15]. Its main advantages are that it is numerically exact (in the statistical sense), that its scaling to multi-orbital models is not bad, and that is easily parallelizable. Among its main drawbacks are the need of analytic continuation that we mentioned, the increased numerical cost to lower the simulation temperature, and the so called “minus sign” problem that prevents the solution of certain multi-orbital problems, especially in the case of cluster methods.

Exact Diagonalization: In this method one adopts a bath of non-interacting fictitious atoms that are coupled to the impurity site. The bath is thus defined by the atomic energies and the coupling amplitudes. Given a set of values for these parameters, a SIAM Hamiltonian is exactly diagonalized by standard techniques and the GF is obtained. The solution is used, via the self-consistency equation (Eq. (13) and 18) to compute the new bath, which is fit to obtain a new set of parameters for the fictitious atoms [1]. The main advantages of this method is that it can be formulated at zero or finite temperature, that it does not pose the problem of analytic continuation, and that its accuracy can be systematically improved. Its drawbacks are that it is numerically costly, especially for multi-orbital models and going to finite temperatures (requires full diagonalization of the Hamiltonian). This is due to the poor scaling of the size of the Hilbert space, which severely limits the number of sites in the bath, typically to about 10, which makes the pole structure of the GF quite discrete. This problem can be overcome by representing the bath with a linear chain and using the DMRG method for the solution [16, 17]. One can implement baths with up to 100 atoms. However, the scaling to multi-orbital models is still poor. We may also mention the solution of the SIAM using Wilson’s NRG method [18]. This approach also allows to implement large atomic baths and provides excellent accuracy at low frequency and zero temperature. Its main shortcoming is, as for DMFT-DMRG, the poor scaling for multi-orbital models moreover it is not particularly advantageous for the study of insulating states.

Iterative Perturbation Theory: The IPT method has both, remarkable advantages and limitations. It is based on a perturbative evaluation to the second order in U/t of the self-energy. The method is very simple and fast. It provided extremely valuable insights on the Mott transition. Its value relies on a fortunate fact, namely, it provides an asymptotically correct solution in the large coupling limit. This is by no means obvious and, apparently, it just works by a lucky stroke. Perturbation theory is by construction good at small coupling, and by no means should be expected to work at large U/t . However, it is not hard to demonstrate it. It is most simply done in the case of a Bethe lattice. We just need to know that, for $0 < \tau < \beta$, $\frac{1}{\beta} \sum_n e^{-i\omega_n \tau} \frac{1}{i\omega_n} = -\frac{1}{2}$, if ω_n is a fermionic Matsubara frequency. From Eq. (18) in the atomic limit ($t = 0$), we see that at half filling $\mathcal{G}_0(i\omega_n) = \frac{1}{i\omega_n}$. Thus, for $0 < \tau < \beta$, we have $\mathcal{G}_0(\tau) = -\frac{1}{2}$ and $\mathcal{G}_0(-\tau) = \frac{1}{2}$. The 2nd order diagram of $\Sigma(i\omega_n)$ therefore takes the value

$$\Sigma^{(2)}(i\omega_n) = -U^2 \int_0^\beta d\tau e^{i\omega_n \tau} [\mathcal{G}_0(\tau)]^2 \mathcal{G}_0(-\tau) = \left(\frac{U}{2}\right)^2 \int_0^\beta d\tau e^{i\omega_n \tau} \mathcal{G}_0(\tau) = \frac{U^2}{4} \frac{1}{i\omega_n}. \quad (20)$$

Using this result and Eq. (14) and (19), we obtain for the G_{loc} in the large- U limit

$$G_{\text{loc}}(i\omega_n) \approx \frac{2}{i\omega_n - (U/2)^2/i\omega_n + \sqrt{(i\omega_n - (U/2)^2/i\omega_n)^2 - D^2}} \quad (21)$$

and from its imaginary part on the real axis we get the DOS

$$\text{DOS}(\omega) \approx \frac{2}{\pi D^2} \sqrt{(\omega - (U/2)^2/\omega)^2 - D^2} \quad \text{with} \quad |\omega - (U/2)^2/\omega| < D \quad (22)$$

which corresponds to two bands of width $\approx D$, split by a gap $\approx U$, where we recall $D = 2t$ is the half-bandwidth of the original non-interacting lattice model, so this solution correctly captures the ‘‘atomic’’ limit of $D \ll U$.

How do we know that it works in between where $U \sim D$? It is because the IPT solution can be benchmarked with the two exact methods that we described before. Comparisons have shown that, quite remarkably, the IPT solution reproduces most of the physical features of the Mott-Hubbard transition at both zero and finite temperature, including the first-order metal-insulator transition that ends in a finite temperature critical point [19, 1]. The surprise gets even bigger: Besides the Hubbard model, the second-order ‘‘recipe’’ for Σ also qualitatively works for the solution of the periodic Anderson model [20] and for the dimer Hubbard model [21]. Unfortunately, the IPT only works at the particle-hole symmetric point. Upon doping the systems, pathological behavior occurs, such as negative compressibility.

In Sec. 4 we provide a link to the IPT source code and propose simple exercises to guide the ‘‘hands-on’’ discovery of the Mott-Hubbard transition.

2.5 Long-range order

DMFT can also be used to explore simple types of magnetic (charge, position, orbital, etc.) long-range ordering, such as ferromagnetic and Néel (i.e. checkerboard) order. In the first case, the equations remain the same, one just needs to consider that the bath may be different for spin up and down. In the case of Néel order, one has to explicitly take into account the two sub-lattices, say A and B. In that case the self-consistency equations read

$$\begin{aligned} \mathcal{G}_{0\sigma}^A(i\omega_n) &= \frac{1}{i\omega_n + \mu - t^2 G_{\sigma}^B(i\omega_n)} \\ \mathcal{G}_{0\sigma}^B(i\omega_n) &= \frac{1}{i\omega_n + \mu - t^2 G_{\sigma}^A(i\omega_n)} \end{aligned} \quad (23)$$

and using the symmetry properties of Néel order between sub-lattices, we get just one equation

$$\mathcal{G}_{0\sigma}(i\omega_n) = \frac{1}{i\omega_n + \mu - t^2 G_{-\sigma}(i\omega_n)}. \quad (24)$$

Note that $G_{\sigma}(i\omega_n)$ is equal to $-G_{-\sigma}^*(i\omega_n)$ in the particle-hole symmetric case, but in general it is not.

3 The Mott-Hubbard transition in DMFT

Before describing the solution of the Hubbard model within DMFT and its relation to the Mott transition, we shall describe some experimental background to motivate this study. The Mott transition is a central problem of strongly correlated systems, and has been occupying a center stage since the discovery of the high T_c cuprate superconductors in the 80's [22], followed by the manganites in the 90's [2], and so on [8]. The interest has been essentially non-stop, with the most recent instance being the fascinating discovery of superconductivity in twisted bi-layer graphene [23]. Once again, this validates the notion that we already discussed in the introduction, namely, that interesting physics always emerges close to a Mott transition. Hence, the relevance of this physical concept.

The Mott transition is a metal-insulator transition (MIT), and the concept goes well before the cuprates, to an argument made by Mott in the 40's [24]. He argued that by considering the dependence of the kinetic and potential energy as a function of the electron density in a solid, one should expect a discontinuous phase transition. In simplest terms the argument is that $E_{\text{kin}} \sim k_F^2/m \sim 1/a^2 \sim n^{2/3}$, while the $E_{\text{pot}} \sim e^2/a \sim n^{1/3}$, so that at low n the E_{pot} dominates, while at large n the kinetic energy does. Hence, as a function of the density, a first order transition should occur between an insulator and a metal. While this argument advances the notion of competition of electronic delocalization versus Coulomb repulsion, which are the ingredients of the Hubbard model, Mott's argument does not immediately apply. What came to be known as the Mott-Hubbard MIT is a phenomenon that occurs at "half-filling," that is, when a band has an occupation of one electron per site (remember that a band has room for two electrons due to the spin), thus, at electronic density $n = 1$. If a band is half-filled, it is partially filled and should have plenty of states just above the Fermi energy. So it should be a metal. Thus, the Mott insulator state is an insulator state that is realized in a half-filled band due to strong Coulomb interactions. Intuitively, if Coulomb repulsion dominates, it will cost a lot of energy to bring two electrons onto the same atomic site. Hence if $n = 1$, the best one can do is to avoid the *double occupation* of any site, which can be achieved by localizing each electron onto a respective atomic site. They would then be locked in their positions, since to move they would have to jump to a neighboring site and that is too costly. Thus, we may think of the Mott state as a global Coulomb blockade.

We should also emphasize that the notion of a Mott transition does not involve a change in the symmetry, such as antiferromagnetic ordering or a lattice dimerization. These two phenomena, associated to the names of Slater and Peierls, can open a gap in the band but do not require strong interactions. Thus, we call them weak-coupling mechanisms, since they emerge from perturbation theory, such as Hartree-Fock. In Fig. 7 we schematically illustrate this point. The ordering effectively doubles the unit cell, thus halving the Brillouin zone (BZ) and doubling the bands that open a gap at the border of the BZ [25].

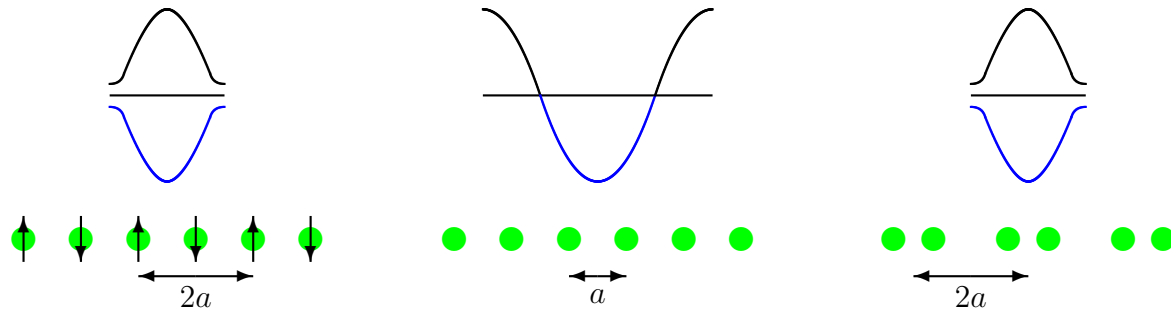


Fig. 7: Schematic representation of the weak-coupling gap opening from the effective lattice parameter doubling $2a$ due to magnetic (left) or lattice (right) symmetry breaking. These mechanisms are associated to Slater and Peierls respectively.

3.1 V_2O_3 a strongly correlated material with a metal-insulator transition

Now we can ask ourselves the question, is the Mott transition realized in nature? Or, is it just an idealized concept? The answer is yes, to both. The Mott transition that we just described is obviously a very idealized and simplified situation: exact half-filling, no change in the symmetry, no disorder, no temperature effect, etc. etc. Yet, and quite remarkably, there seems to be a realization of the Mott-transition concept in the compound V_2O_3 . In Fig. 8 we show the phase diagram of this famous compound. We observe three phases, an antiferromagnetic insulator (AFI) at low temperature, and two paramagnetic phases at intermediate temperatures, one insulator (PMI) and one metallic (PMM) that are separated by a first-order line, which ends in a critical point (CP). The important feature is that the MIT occurs with no change in lattice symmetry. It can be driven by temperature or by pressure (hydrostatic or chemical). The small Cr and Ti substitution is considered to slightly change the lattice spacing, hence the bandwidth, but not the number of carriers. In fact, the no change in the lattice symmetry is easily understood from the fact that if one starts, say in the PMI next to the first-order line, and then heats-up the system just above the CP, then applies pressure just past the CP, and cool down again, one arrives to the qualitatively different PMM phase, all through a continuous and smooth process. This feature shows that the MIT in V_2O_3 is qualitatively similar to the familiar liquid-vapor transition in water.

The study of the MIT in V_2O_3 continues to be a matter of strong scientific interest, attention and debates with many interesting findings that continuously challenge our physical understanding of this compound. Among the most recent and exciting discoveries is that strong electric pulsing may collapse the Mott insulating state and that the phenomenon may be exploited to implement *artificial neurons* [26–28]. From a conceptual point of view understanding this new and unexpected *neuromorphic functionality* [29] poses a significant challenge, namely to describe the Mott transition out-of-equilibrium. This is a topic of great current interest [30], which is also motivated by the fast development of so called “pump-probe” experiments.

After this brief introduction to the Mott phenomenon and its relevance, we now move on to describe the Mott-Hubbard transition within DMFT.

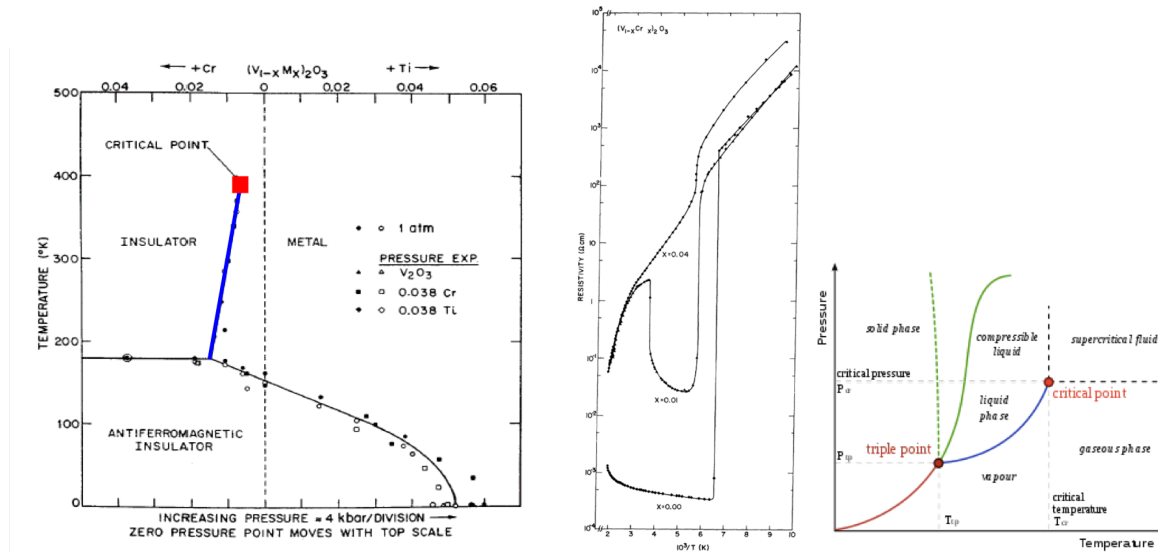


Fig. 8: Left: Phase diagram of V_2O_3 . Negative and positive chemical pressure can be applied with a few % of Cr and Ti substitution. The blue line indicates the first-order line between the metal and the insulator within the paramagnetic phase. The orange square indicates the second-order critical end-point. Center: Resistivity of V_2O_3 across the meta-insulator transitions. Right: A similar first-order line and critical end-point are present in the familiar water-vapor phase transition.

3.2 The Mott-Hubbard transition

As mentioned before, the Mott insulator is realized at half-filling, i.e., one electron per site in a mono-atomic lattice. From experiments, we observe that the transition can be driven by changing the bandwidth, i.e., applying pressure, and by heating. Thus, in the framework of a Hubbard model, which can be considered as a minimal model to capture the physics, one may explore the behavior at half-filling and as a function of the ratio of interaction to bandwidth (U/W), temperature (T), and doping (δ) away from half-filling, i.e., $\delta = n - 1$. For simplicity, we shall consider the case of a Bethe lattice with a semicircular DOS. We shall adopt as unit of energy of the problem the half-bandwidth $D = W/2$ that we set equal to one, unless indicated. As we discussed before, to study the Mott transition as observed in Cr-doped V_2O_3 , we need to restrict ourselves to paramagnetic (PM) states. However, the solution of the Hubbard model on a bipartite lattice, such as Bethe or the (hyper-)cubic, has strong “Néel nesting” that favors an AFI state at low T . Thus, we shall ignore for the moment antiferromagnetic solutions and only be concerned with paramagnetic ones, and we shall explore whether Coulomb repulsion can lead to the break down of a metallic state in the half-filled band of a tight-binding model. In Fig. 9 we show the beginning of the answer to this question within DMFT. We show the evolution of the DOS of a half-filled tight-binding model on a Bethe lattice at $T = 0$ as the interaction U is increased.

The main feature of the solution is the existence of a MIT as a function of increasing interaction strength U . We observe that the $DOS(\omega = 0)$ is finite at low U , but becomes zero when an insulating gap opens at large U . We can look at the nature of this evolution in more detail. We

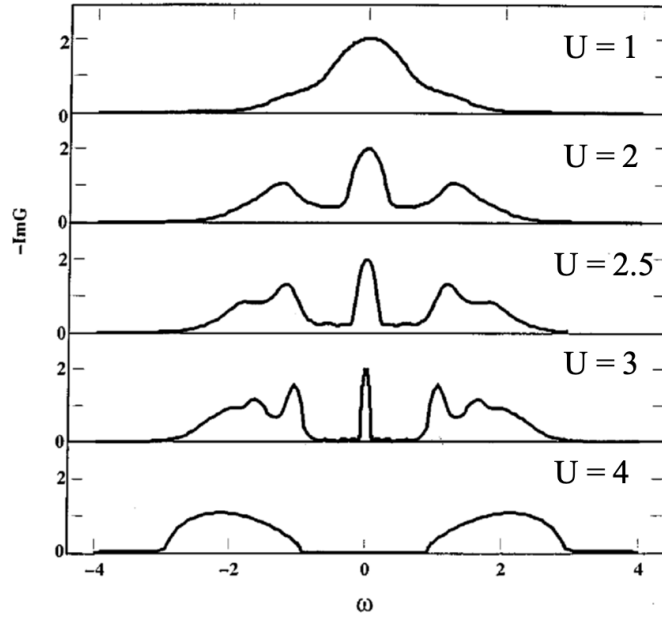


Fig. 9: $DOS(\omega)$ of the HM at $T = 0$ for increasing values of U . The quasiparticle peak narrows as U increases until it collapses at the critical value U_{c2} . From [31].

observe that there is a peak developing at low frequency which becomes increasingly narrow. This is called the quasi-particle peak and its origin can be connected to the Kondo physics we discussed in the introduction. The narrowing of the peak corresponds to an increase of the effective mass as the MIT is approached. A detailed numerical study shows that the effective mass goes as $m^* \sim 1/Z \sim (U_{c2} - U)$, where Z is the quasiparticle residue, i.e., the spectral intensity of the peak, that we defined before, and $U_{c2} \approx 3D$ is the critical value of the interaction where the MIT occurs. The other feature that we observe is the growth of two large peaks with the spectral weight that is lost from the central peak (i.e. $1 - Z$) at frequencies $\pm U/2$. After the transition only these two peaks are left and are separated by a charge gap $\Delta \approx U - 2D$. They are called the Hubbard bands.

3.3 Band-structure evolution across the metal-insulator transition

It is interesting to go back to the lattice to observe what is the nature of the electronic states that conform these peaks. In the case of a Bethe lattice the notion of momentum space is not obvious, so instead of labelling the single-particle states by their momentum quantum number we shall use their single particle energy ε . So the dispersion relation of the interacting energies that is usually denoted by $E = E(k)$ with $k \in BZ$ becomes $E = E(\varepsilon)$ with $\varepsilon \in [-D, D]$. So, Eq. (16) becomes

$$G(\varepsilon, i\omega_n) = \frac{1}{i\omega_n - \varepsilon - \Sigma(i\omega_n)} \quad (25)$$

In the non-interacting case $U = 0$ and $\Sigma = 0$. Then, the GF has poles at ε and the non-interacting dispersion is simply linear with $E(\varepsilon) = \varepsilon$ and $\varepsilon \in [-D, D]$. One intuitive way to

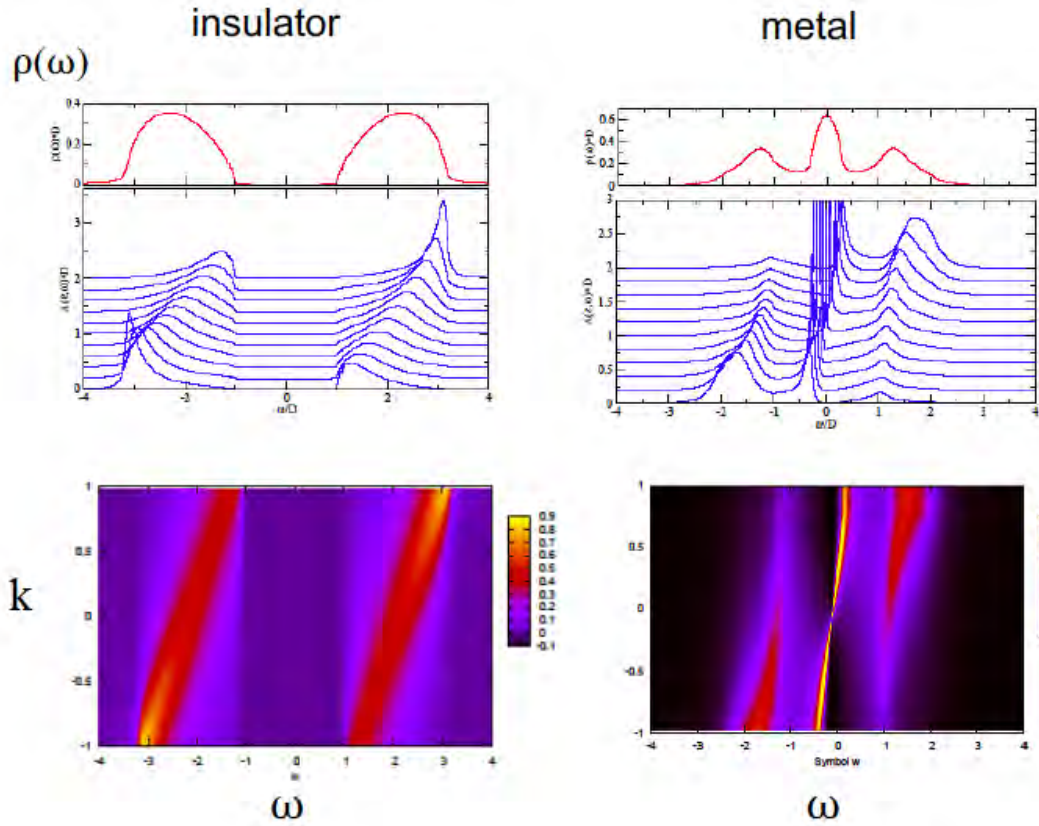


Fig. 10: Top: DOS of the HM at $T = 0$ for the Mott insulator $U > U_{c2}$ (left) and the correlated metal $U < U_{c2}$ (right). Middle: $A(\varepsilon, \omega)$ for increasing values of $\varepsilon \in [-D, D]$. Bottom: Idem in a color intensity plot (the label k plays an analogous role as ε denoting the quantum number of the non-interacting single-particle states (see text)).

think of this band structure is that it is qualitatively similar to that of a 1D tight binding model, i.e., a linearized $-\cos(k)$. Thus, the state $\varepsilon = -D$, with $E(-D) = -D$ is the bottom of the band, i.e., often the Γ -point; the state $\varepsilon = +D$ with $E(+D) = +D$ is the top of the band and the edge of the BZ; and the state $\varepsilon = 0$ with $E(0) = 0$ is the Fermi energy. From Eq. (25) we clearly see that the self-energy function encodes the interaction effects, as it modifies the pole structure of the non-interacting GF and also broadens the poles giving a finite lifetime to the electronic states. In Fig. 10 we show the spectral functions $A(\varepsilon, \omega) = -\text{Im} G(\varepsilon, \omega)/\pi$ of the interacting model for the strongly correlated metal and for the insulator. The $\omega < 0$ spectral functions are measured in ARPES photoemission experiments.

We observe various features which are worth pointing out. In the case of the metal we observe that the pole structure at low energy remains a collection of sharp resonances with a linear dispersion. This indicates that the metallic states are well defined quasi-particle states (i.e., have long life-times) and that their mass is enhanced by the effect of interactions. The effective mass is larger because the band is flatter, as it disperses linearly between $[-ZD, +ZD]$, where we recall that the quasiparticle residue $Z < 1$. Thus, heavy mass aside, the states are qualitatively similar to Bloch waves and we call these states *coherent*. We also observe the Hubbard bands developing at higher frequency. While they show dispersive features, the nature of the propagation that they describe is very different. The electronic states are broad in energy,

which indicates that the excitations are rather short-lived and the propagation of the electrons is *incoherent*. In other words, they describe rather localized particle-like states that are qualitatively different from momentum eigenstates. This correlated metallic state is perhaps the most profound physical insight that emerged from DMFT. We see that the solution of the Hubbard model within DMFT is a concrete realization of a quantum many-body electronic state which simultaneously shares both, wave-like and particle-like features [32].

The Mott-Hubbard insulator has only incoherent Hubbard bands with a dispersion that resembles the non-interacting dispersion, but split by the Coulomb repulsion U , thus approximately follows $E(\varepsilon) = \pm \frac{U}{2}\varepsilon$. We note that the lifetime has a non-trivial variation across the BZ, with a more quasiparticle-like character at the bottom and top of the lower and upper Hubbard bands respectively, and becomes more incoherent close to the gap edges.

3.4 Coexistence of solutions and the first-order transition line

Another remarkable feature of the MIT is the coexistence of solutions. In Fig. 9 we showed the evolution of the DOS(ω) as the interaction U is increased, which displays a MIT at a critical value U_{c2} . However, this is not the only transition. If one starts from the insulator at large U and reduces the interaction one observes that the two Hubbard bands get closer and the gap $\Delta \approx U - 2D$ shrinks. The remarkable feature is that this insulating solution continues to exist for $U < U_{c2}$. The solution eventually breaks down at a value $U_{c1} \approx 2D$, where the gap closes. Thus, for $U \in [U_{c1}, U_{c2}]$ two qualitatively different solutions one metallic the other insulating coexist. This feature can be considered analogous to the coexistence of solutions in the MFT of the ferromagnetic Ising model, with all-up and all-down.

There are many consequences that follow from this feature. If keeping the occupation fixed at $n = 1$, at particle-hole symmetry, and increasing the temperature, the solutions will not disappear. They smoothly evolve, giving rise to a coexistence region in the U - T plane. The evolution of the two solutions with increasing T is qualitatively different.

The metallic one has a low frequency quasiparticle peak. Its width can be related to the Kondo energy scale of the associated impurity problem. This sets a dynamically generated new low-energy scale in the system, much smaller than D (i.e. t) and U . As T is increased, the Kondo resonance can no longer be sustained and the dynamical singlet state that the impurity forms with the bath is broken. The energy scale of the quasiparticle peak is $\sim (U_{c2} - U)$, thus we may expect that the correlated metallic solution will break down along a line $U_{c2}(T_{MIT})$, with T_{MIT} being proportional to $(U_{c2}(0) - U)$. This expectation is indeed realized as shown in Fig. 11. Near U_{c2} there is a significant magnetic moment due to the penalizing effect of U on the probability of double occupation. Moreover, above the line $U_{c2}(T)$, the temperature is too large for the moment to be Kondo screened and we are left with an incoherent collection of disordered magnetic moments at each lattice site.

On the other hand, as T is increased in the insulating solution, the gap may get thermally filled without any significant effect. Thus we may expect that the coexistence region in the U - T plane has a triangular shape, which is actually the case as shown in Fig. 11. The figure also indicates

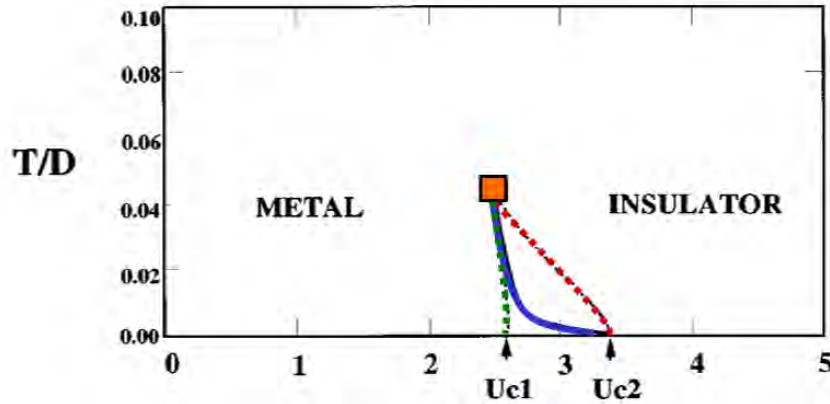


Fig. 11: Phase diagram in the U - T plane. The dotted lines show the region where the paramagnetic metallic and insulating solutions coexist. The red dotted line is $U_{c2}(T)$ and the green dotted line is $U_{c1}(T)$. The blue line denotes the first-order transition where the free energies of the two solutions cross. The orange square denotes the finite- T critical end-point.

the line where the free energies of the two solutions cross, which denotes a first order metal-insulator transition in this model. The fact that the metal is more stable at low T , due to the additional energy gain of the Kondo state, implies also that the physical transition is from a metal to an insulator upon heating. This is qualitatively the case in the MIT within the paramagnetic phase of V_2O_3 that we discussed before. We should perhaps remark here that there is another vanadate, VO_2 , that also displays a transition driven by temperature between two paramagnetic states. However, in that case and contrary to V_2O_3 , the transition is from an insulator to a metal upon heating. Thus the two transitions are qualitatively different. Nevertheless, one may also understand the transition in VO_2 as a Mott transition with a two-site quantum impurity, where the insulating ground-state wins as the two moments screen each other into a local singlet. Such an insulator-metal transition has been discussed recently [33, 21, 34].

3.5 Endless directions

We have described the core of the Mott transition physics that was unveiled by the introduction of the DMFT approach formulated as a mapping of the (infinite-dimensional) lattice problem onto a self-consistent quantum impurity [35–37, 31]. From that starting point an endless number of problems and extensions have been explored and continue to be developed. We shall briefly mention some of them here.

3.5.1 Doping driven Mott transition

In this lecture we have investigated the MIT at half-filling keeping one electron per site. The system is at particle-hole (p-h) symmetry, hence the $DOS(\omega)$ are always even functions. In this situation we have seen that if the interaction U is strong enough and the temperature T low enough the system is in a Mott insulator state. We can destabilize this insulator state by *doping* the system, i.e., by changing the particle occupation by δ . This can be done by changing the chemical potential away from the p-h symmetry at $\mu = U/2$. In the simple single band

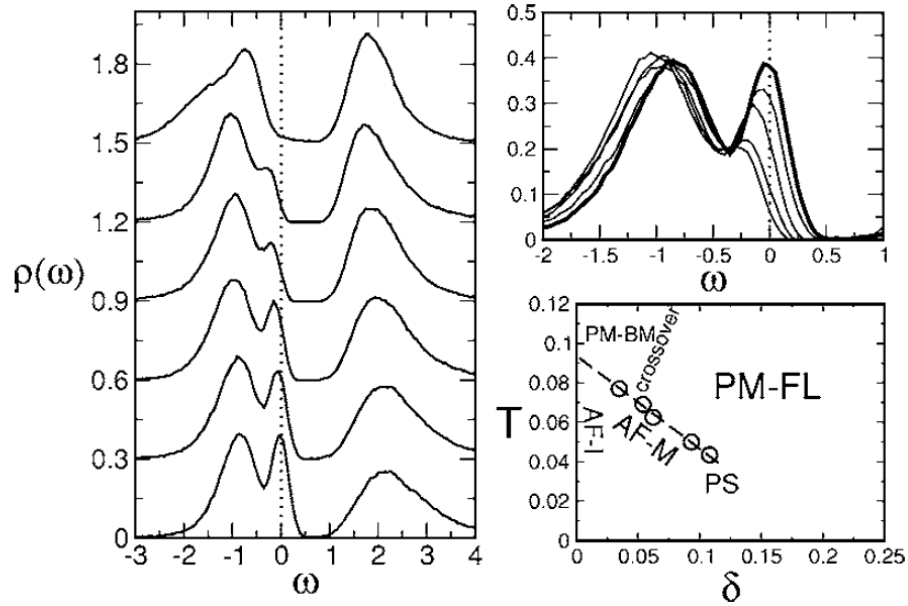


Fig. 12: Left: Paramagnetic $DOS(\omega)$ of a lightly hole-doped Hubbard model at $U = 3.125$, $T = 0.1$, and increasing $\delta = 0.003, 0.0076, 0.0114, 0.022, 0.038$, and 0.055 , from top to bottom. Top right: Detail of the evolution of the quasiparticle peak in the previous results. Bottom right: Phase diagram as a function of δ and T for $U > U_{c2}$. From [38].

Hubbard model that we consider it is equivalent to dope particles or holes, the resulting GFs are related by the change $\omega \rightarrow -\omega$. The effect of doping is to create a correlated metallic state. It shares several features of the $n = 1$ correlated metal that we have already described. It has a narrow quasiparticle peak at $\omega = 0$ that is flanked by the two Hubbard bands. The spectral intensity of the quasiparticle peak is in this case controlled by the doping, with $Z \approx 1/\delta$. Thus the renormalized bandwidth is $\sim \delta D$. This is again a small energy scale and increasing the temperature will destroy the quasiparticle peak. The way this takes place is qualitatively different from the p-h symmetric case. As shown in Fig. 12 one observes that the quasiparticle peak becomes very asymmetric with respect to the origin. This signals a departure from the Fermi liquid state and is associated to the notion of *resilient quasiparticles* and of *bad metal* states [38]. In a bad metal state the system has spectral weight at the Fermi energy but the quasiparticles have very short lifetimes or, equivalently, very large scattering rates that lead to a resistivity in excess of the Ioffe-Regel limit. In other words the mean-free path becomes shorter than the lattice spacing. This feature is often observed in strongly correlated systems including the metallic phase of the vanadates that we mentioned before and the high- T_c cuprate superconductors.

By a continuity argument one should also expect that the coexistence region of solutions must extend into the non p-h symmetric case for $\mu \neq U/2$. This feature has been investigated in [39] where the main consequence was the finding of a divergence in the electronic compressibility. This electronic anomaly can be considered as a precursor for charge density waves, phase separation, and lattice structural changes [40].

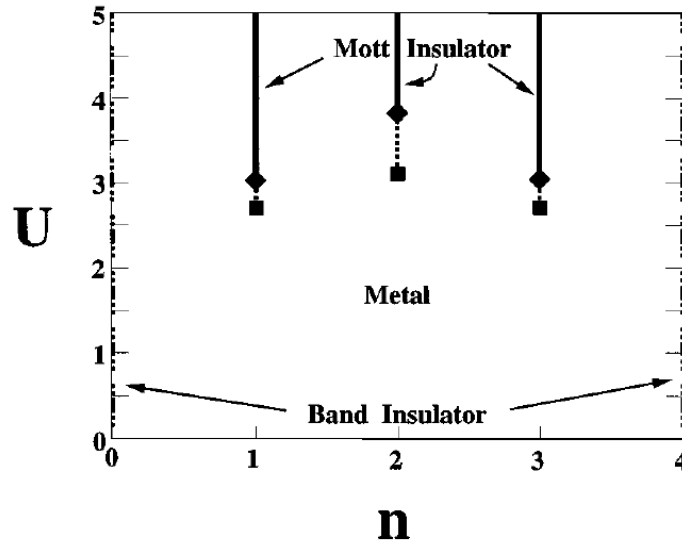


Fig. 13: Phase diagram of the 2-orbital degenerate band Hubbard model. See Fig. 2 for comparison. From [43].

3.5.2 Mott-Hubbard transition in the presence of long-range order

So far we have been mostly concerned with the paramagnetic state. In Sec. 2.5 we described how DMFT can be extended to consider phases with LRO, such as Néel antiferromagnetism. In fact, the lowest energy solution of the Hubbard model at half-filling and $T = 0$ in bipartite lattices, such as Bethe or the hyper-cubic, is an antiferromagnetic insulator (AFI). This state is the most stable below an ordering temperature T_N , which depends on the value of U . At small U the AFI state can be considered as a Slater AF, with a T_N and a gap Δ that are both small, and grow exponentially with U . This state is rather well captured by Hartree-Fock MFT. In contrast, at high values of U , the electrons are Mott localized and the AFI should be considered as a Heisenberg AF where the ordering follows from the super-exchange interaction $J = 4t^2/U$. In this case, the gap is large and $\sim U$, while the $T_N \sim J$, so it decreases with increasing U . This situation is realized in high- T_c superconductors, which have a large gap \sim eV and a T_N one or two orders of magnitude smaller.

An interesting issue is to explore the behavior of the model when one dopes away from the half-filled AF Mott insulator. Despite a significant amount of work done in DMFT, there are few studies that consider this question in the Hubbard model and the detailed evolution remains rather poorly known [38]. From those studies the physical picture that emerges is that of a heavy-mass renormalized quasiparticle band at low frequencies, which is split in two due to the effective doubling of the lattice periodicity. These coherent bands are flanked by Hubbard bands, which are separated by an energy $\sim U$ and have different spectral intensities for the up and down spin projections. Interestingly, these features are qualitatively similar to those obtained in solutions of Cluster DMFT calculations, which unlike “standard” DMFT incorporate spatial spin fluctuations [41, 42].

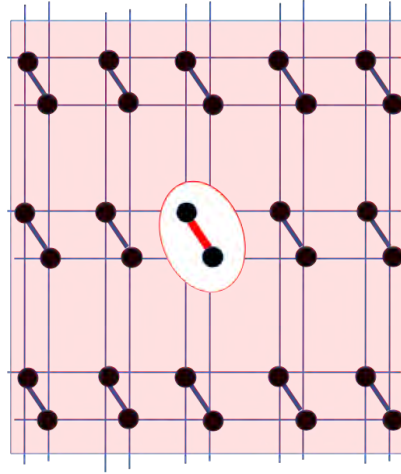


Fig. 14: Schematic representation of the embedding of a dimer (cluster) in the DHM. This model can be considered the simplest instance of CDMFT.

3.5.3 Multi-orbital models

DMFT can be naturally extended to consider atomic sites with multiple orbitals that lead to multiple bands. This was initially done for the simplest case of two orbitals with identical hopping amplitudes that leads to two degenerate bands [43]. In Fig. 13 we show the phase diagram in the U - n plane. The interesting feature is that for an N -orbital Hubbard model, Mott transitions are found for fractional dopings $n/2N$ with $n = 1, \dots, 2N-1$, which extends the notion of half-filling to the multi-orbital case. The intuitive way to think about this is that Mott states are found when there is an integer filling of electrons at a lattice site. The energy to add an extra electron to the lattice, would be the Coulomb charging energy $\sim U$. Interestingly, the correlated metal and insulator states are qualitatively similar to those at half-filling, presenting Hubbard bands and heavy quasiparticle bands. Moreover, Mott transitions also have regions of coexistence and therefore the MITs have first order character.

One novelty that the multi-orbital models incorporate is the Hund interaction. This is responsible for the FM alignment of electrons occupying the same atomic site, creating large local magnetic moments as in the colossal magnetoresistive manganites [2]. The large magnetic moment is more difficult to screen, leading to a decrease of the Kondo temperature of the associated impurity model. This has as a consequence the emergence of correlated metallic states with low coherence temperatures and bad metallic features [44, 45]. These systems are known as Hund's metals and their study is relevant for correlated materials like the iron based superconductors [46].

3.5.4 Cluster DMFT

Since DMFT is exact in the limit of ∞ - d , where the lattice problem is mapped to a single impurity by taking one site and embedding it in a self-consistent environment, a natural extension is to consider the embedding of a small portion of the lattice, or a cluster. Such approaches go by the name of cluster-DMFT (CDMFT) [47] and dynamical cluster approximation (DCA) [48].

In the first case one defines a cluster of atoms in real space and embeds it in an effective self-consistent medium, pretty much as we have described before (Sec. 2.2). This is schematically illustrated for the case of a lattice of dimers in Fig. 14. The dimer Hubbard model (DHM) can be exactly solved within CDMFT method [49, 33], and has recently been considered for the interpretation of experiments in VO_2 . However, when applied to general lattices there are certain technical difficulties to restore translational invariance and different approximate schemes have been proposed.

The DCA method is formulated in reciprocal space. It is based on computing a coarse grained self-energy of a finite cluster, i.e., in a space of discrete momentum K , which is then used to obtain estimates of the actual infinite-lattice self-energy (where the momentum k is continuous). Thus the method is fully formulated in momentum space, including the generalization of $\mathcal{G}_0(i\omega_n)$ to a $\mathcal{G}_0(K, i\omega_n)$. So the issue of restoring translational invariance does not emerge. However, there is a price to pay, which is the discontinuity of the self-energy that is defined of coarse-grain “patches” of the BZ.

Both extensions of DMFT enable the exploration of momentum dependence. One of the main results that these approaches provided is the notion of momentum-space differentiation. Namely, the possibility that a Mott gap may open only in certain regions of the Fermi surface. This provides an interpretation to the intriguing observation of “Fermi arcs” in the cuprates [50].

3.5.5 Realistic DMFT or LDA+DMFT

DMFT has also been extended to incorporate real material-specific information. This methodology goes by the names of DFT+DMFT, LDA+DMFT, or Realistic-DMFT [47]. Schematically, the approach retains the same mapping onto an QIP and its self-consistent solution, but the material-specific electronic structure dispersion replaces the ε_k in the k -summations, Eq. (13). Since LDA solution to the DFT equations is a self-consistent method itself, this opens the door to a variety of possible schemes. We shall not dwell further on this topic since there is the dedicated lecture by E. Pavarini.

3.5.6 Out-of-equilibrium Mott transition

An exciting new frontier is the investigation of the correlated systems driven away from equilibrium conditions. This is relevant for recently developed experimental techniques such as “pump-probe” spectroscopies that give access to the time-resolved evolution of a strongly interacting quantum material. Particularly interesting to us is the possibility of driving a Mott insulator out of equilibrium, which has been considered in a variety of experimental studies. Here we cite some particularly interesting ones related to vanadates [51, 52] that indicate that a sharp insulator-metal transition (IMT) can be induced by strong enough light irradiation. Particularly interesting is that these experiments seem to have provided strong evidence of the meta-stable states (i.e. the state coexistence) that has been predicted by DMFT studies of the Hubbard and dimer Hubbard models. The latter case is particularly interesting is where a photoemission study of the Mott insulator VO_2 was conducted [53]. The main observations where

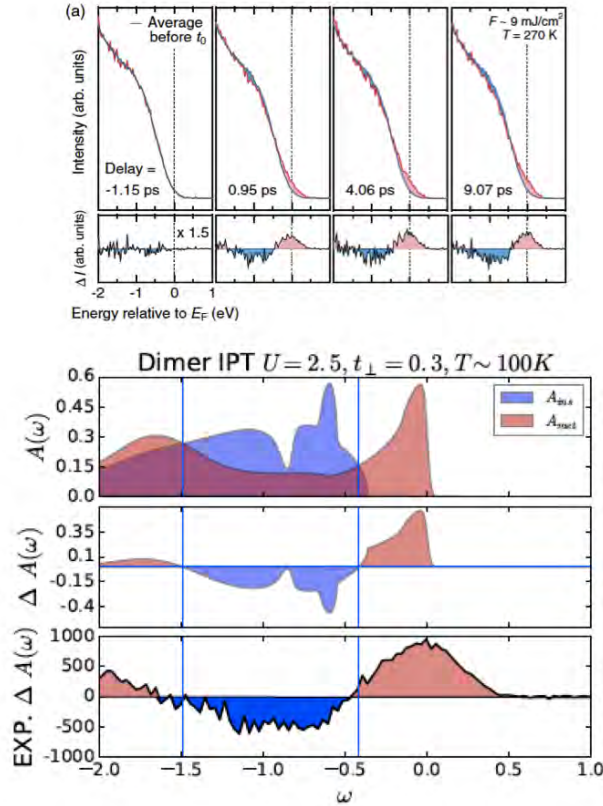


Fig. 15: Top: Photoemission spectra of the VO_2 insulator “before and after” the pump pulse. Bottom: Difference between after- and before-pump spectra showing the transfer of spectral intensity across the pump-driven Mott transition. Mid-top: Occupied part ($\omega < 0$) of the $\text{DOS}(\omega)$ of the insulator (blue) and metal (red) coexistent solutions of the DHM. Mid-bottom: Difference between the model $\text{DOS}(\omega)$. Bottom: Detail of experimental photoemission difference data.

the existence of a sharp light-fluence threshold for the IMT, that the resulting metallic state was very long lived (> 10 ps) and that the photoemission spectrum was different from the high- T metallic state. We found that this intriguing metallic state could be the realization of a *monoclinic* metal in VO_2 , which emerges from a DMFT study of the Mott insulating state of a dimer Hubbard model [33, 21, 34]. In Fig. 15 we show the experimental variation of the spectrum across the IMT along with the results from the theoretical study [54]

The time-resolved behavior across the Mott-Hubbard transition can be studied by extending the DMFT approach to the out-of-equilibrium situation by adopting the Kadanoff-Baym and Keldysh GFs formalism. These extension of DMFT received a great deal of attention in recent years [55, 30]. Despite significant progress and new insights the detailed solution of the problem in the coupling regime where there are coexistent solutions still remains a challenge. We shall not devote much more here and point to the lecture on this topic by J. Freericks.

3.5.7 Mottronics for Artificial Intelligence

One of the latest and perhaps most original and exciting developments regarding the Mott transition is the possibility of using the Mott insulators to fabricate artificial electronic neurons for spiking neural networks [28]. This is particularly timely given the current explosion and inter-

est in artificial intelligence (AI). The algorithms of AI are often based on neural networks (NN) such as the classic Hopfield model, popular in the 70's, to the more modern convolutional NN. In general, NN have two types of units, a non-linear input-output device, the neuron, and devices that interconnects the neurons and modulate the intensity of their coupling, the synapses. Models of NN can be implemented in software or in hardware. In the first case, a notable example is the AlphaGo code that has defeated the world champion of Go [56]. However, running this algorithm requires a powerful supercomputer that consumes several kW. In the second case, powerful chips are built using state-of-the-art electronics that can implement a million neurons, such as TrueNorth [57]. They are energetically efficient but their main limitation is that they require almost 10^{10} transistors to implement a million neurons (synapses require relatively fewer transistors than neurons). While this accomplishment is remarkable, these chips are still several orders of magnitude below the 10^9 neurons in a cat's brain. This situation opens the way for a disruptive technology, which may implement artificial neurons using far fewer components.

Recently, we have shown that a Mott insulator may accomplish this task [58, 29]. The key finding was that Mott insulators under electric pulsing realize a *neuromorphic functionality*, which consists in behaving analogously to the leaky-integrate-and-fire (LIF) model of spiking neurons [59]. The LIF model is a classic and basic model of biological neurons. It describes the integration of electric input that arrives at a neuron through its dendrites, the leakage during the time in-between arriving input spikes, and the fire of an action potential when the integrated input reaches a threshold. A Mott insulator under electric pulsing may behave similarly. The key feature is that in narrow gap Mott insulators, such as GaTa_4Se_8 [60] or V_2O_3 , when a strong voltage is applied, creating a field of the order of kV/cm, a collapse of the resistance is observed after a certain delay time $\tau_d \sim$ tens of μs [61]. Let us now consider applying instead of a constant voltage a train of pulses, where the duration of each pulse τ_p is smaller than τ_d . It is easy to understand that if the time between the pulses τ_w is very long, then each pulse is an independent perturbation that will not produce the resistive collapse of the Mott state. On the other extreme, if τ_w goes to zero, then the pulses will simply accumulate and produce the collapse after n_{sw} pulses, where $n_{sw}^{min} = \tau_d/\tau_p$. Thus, n_{sw} is a function of τ_w that increases from n_{sw}^{min} to ∞ . This behavior was originally predicted by a phenomenological model of resistive breakdown in Mott insulators and experimentally observed [61], as illustrated in Fig. 16.

The phenomenological model consisted of a resistor network, where the key assumption for the resistive units was the existence of two resistive states. One more stable with high resistance and a metastable one with low resistance. This assumption was motivated by the coexistence of solutions of the DMFT studies of Hubbard models that we described in this lecture. Interestingly, the equations that describe the resistor network model can be shown to be analogous to that of the LIF model of neurons [29], where the role of spikes is played by the applied pulses. The “firing” of an action potential corresponds to the current spike through the Mott insulator as its resistance collapses.

Interestingly, following a different line of work a group at Hewlett-Packard has proposed an implementation of another classic biological neuron model, the Hodgkin-Huxley model [59], using NbO_2 , which is also a Mott insulator material [62].

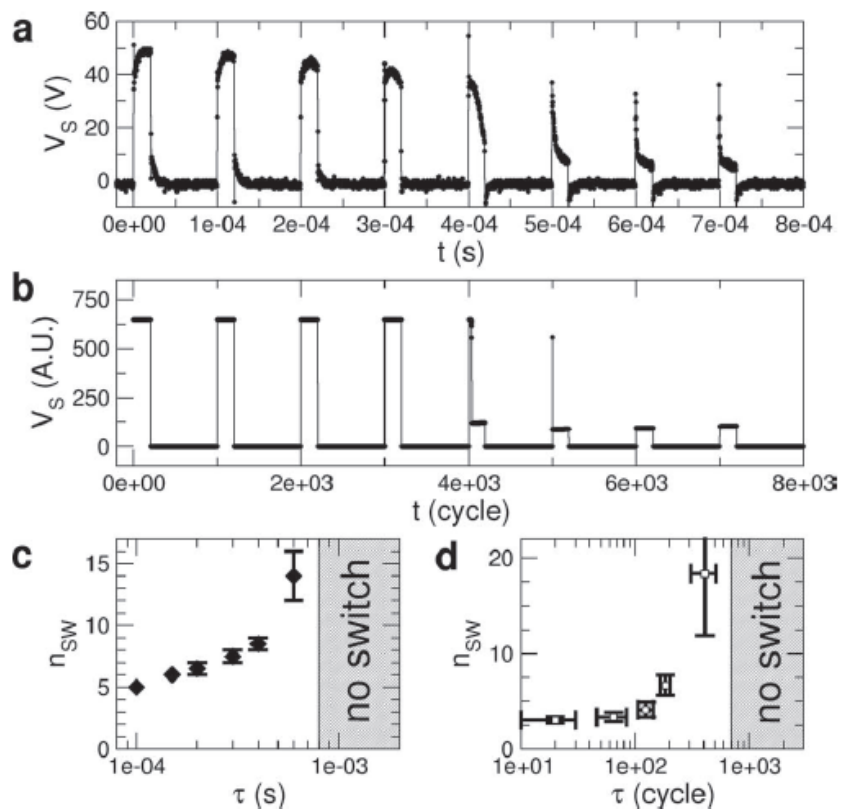


Fig. 16: *Top: Collapse of the Mott insulator state in GaTa_4Se_8 observed after 5 pulses by the collapse of the resistance (i.e., the voltage drop on the sample). Middle: Resistor network model simulation that qualitatively captures the behavior of the Mott insulator under strong electric pulsing. Bottom: Systematic behavior of n_{sw} as a function of the time between pulses τ_w (left is experimental data and right model simulations). From [61].*

Thus the neuromorphic functionalities of Mott insulators, owing to the unique non-linear behavior of their I - V characteristics, are emerging as a new and exciting road towards bringing Mott materials to the realm of future electronics — or rather *Mottronics*.

4 Hands-on exercise (with IPT code): The Mott-Hubbard transition

Many of the plots in this lecture illustrating the Mott-Hubbard transition were obtained by solving the DMFT equations using an impurity solver based on iterative perturbation theory (Sect. 2.4) [35, 31]. This approximate method has the advantage of being simple and providing qualitatively good solutions across the transition. The interested reader is invited to download the IPT codes and go through the proposed exercises that serve as a guide for a hands-on exploration of the Mott-Hubbard metal-insulator transition in DMFT. Codes are available for free at <http://mycore.core-cloud.net/index.php/s/oAz0lIWuBM90Gqt>.

References

- [1] A. Georges, G. Kotliar, W. Krauth, and M. Rozenberg, *Rev. Mod. Phys.* **68**, 13 (1996)
- [2] E. Dagotto, *Science* **309**, 257 (2005)
- [3] B.J. Kim *et al.*, *Science* **323**, 1329 (2009)
- [4] V. Brouet *et al.*, *Phys. Rev. B* **92**, 081117(R) (2015)
- [5] H. Alloul, *EPJ Web of Conferences* **23**, 00015 (2012)
- [6] P. Wzietek *et al.*, *Phys. Rev. Lett.* **112**, 066401 (2014)
- [7] A. Fujimori, *J. Phys. Chem. Solids* **53**, 1595 (1992)
- [8] M. Imada, A. Fujimori, and Y. Tokura, *Rev. Mod. Phys.* **70**, 1039 (1998)
- [9] G. Mahan: *Many-Particle Physics*, (Springer, New York, 2000)
- [10] J.W. Negele, and H. Orland: *Quantum Many-particle Systems* (Perseus, 1998)
- [11] W. Metzner and D. Vollhardt, *Phys. Rev. Lett.* **62**, 324 (1989)
- [12] E. Gull *et al.*, *Rev. Mod. Phys.* **83**, 349 (2011)
- [13] O. Parcollet, M. Ferrero, T. Ayrál, H. Hafermann, I. Krivenko, L. Messio, and P. Seth, *Comp. Phys. Comm.* **196**, 398 (2015)
- [14] J.E. Hirsch and R.M. Fye, *Phys. Rev. Lett.* **56**, 2521 (1986)
- [15] E. Gull, A.J. Millis, A.I. Lichtenstein, A.N. Rubtsov, M. Troyer, and P. Werner, *Rev. Mod. Phys.* **83**, 349 (2011)
- [16] D.J. García, K. Hallberg, and M.J. Rozenberg, *Phys. Rev. Lett.* **93**, 246403 (2004)
- [17] D.J. García, E. Miranda, K. Hallberg, and M.J. Rozenberg, *Phys. Rev. B* **75**, 121102(R) (2007)
- [18] R. Bulla, T.A. Costi, and T. Pruschke, *Rev. Mod. Phys.* **80**, 395 (2008)
- [19] G. Kotliar, E. Lange, and M.J. Rozenberg, *Phys. Rev. Lett.* **84**, 5180 (2000)
- [20] M.J. Rozenberg, G. Kotliar, and H. Kajueter, *Phys. Rev. B* **54**, 8452 (1996)
- [21] O. Nájera, M. Civelli, V. Dobrosavljević, and M.J. Rozenberg, *Phys. Rev. B* **97**, 045108 (2018)
- [22] B. Keimer, S.A. Kivelson, M.R. Norman, S. Uchida, and J. Zaanen, *Nature* **518**, 179 (2015)

-
- [23] Y. Cao *et al.*, Nature **556**, 80 (2018)
- [24] N. Mott: *Metal-Insulator Transitions* (Taylor & Francis, 1997)
- [25] N.W. Ashcroft and N. Mermin: *Solid State Physics* (Brooks, 1976)
- [26] I.H. Inoue and M.J. Rozenberg, Adv. Funct. Mat. **18**, 2289 (2008)
- [27] E. Janod *et al.*, Adv. Func. Mat. **25**, 6287 (2016)
- [28] J. del Valle, G. Ramírez, M.J. Rozenberg, and I.K. Schuller, Jour. Appl. Phys. **124**, 211101 (2018)
- [29] P. Stoliar *et al.*, Adv. Funct. Mat. **27**, 1604740 (2017)
- [30] H. Aoki, N. Tsuji, M. Eckstein, M. Kollar, T. Oka, and P. Werner, Rev. Mod. Phys. **86**, 779 (2014)
- [31] X.Y. Zhang, M.J. Rozenberg, and G. Kotliar, Phys. Rev. Lett. **70**, 1666 (1993)
- [32] M. Takizawa *et al.*, Phys. Rev. B. **80**, 235104 (2009)
- [33] O. Nájera, M. Civelli, V. Dobrosavljević, and M.J. Rozenberg, Phys. Rev. B **95**, 035113 (2017)
- [34] H.T. Stinson *et al.*, Nat. Commun. **9**, 3604 (2018)
- [35] A. Georges and G. Kotliar, Phys. Rev. B **45**, 6479 (1992)
- [36] M. Jarrell, Phys. Rev. Lett. **69**, 168 (1992)
- [37] M.J. Rozenberg, X.Y. Zhang, and G. Kotliar, Phys. Rev. Lett. **69**, 1236 (1992)
- [38] A. Camjayi, R. Chitra, and M.J. Rozenberg, Phys. Rev. B Rapid Comm. **73**, 041103 (2006)
- [39] G. Kotliar, S. Muthry, and M.J. Rozenberg, Phys. Rev. Lett. **89**, 046401 (2002)
- [40] S.R. Hassan, A. Georges, and H.R. Krishnamurthy, Phys. Rev. Lett. **94**, 036402 (2005)
- [41] L. Fratino *et al.*, Phys. Rev. B **96**, 241109(R) (2017)
- [42] S. Sakai *et al.*, Phys. Rev. Lett. **111**, 107001 (2013)
- [43] M. Rozenberg, Phys. Rev. B **55**, 4855(R) (1997)
- [44] A. Georges, L. de' Medici, and J. Mrarlje, Annu. Rev. Condens. Matter Phys. **4**, 137 (2013)

- [45] L. de' Medici: *Hund's Metals Explained*, in E. Pavarini, E. Koch, R. Scalettar, and R. Martin (eds.): *The Physics of Correlated Insulators, Metals, and Superconductors Modeling and Simulation Vol. 7* (Forschungszentrum Jülich, 2017) <http://www.cond-mat.de/events/correl17>
- [46] Z.P. Yin, K. Haule, and G. Kotliar, *Nat. Mater.* **10**, 932 (2011)
- [47] G. Kotliar *et al.*, *Rev. Mod. Phys.* **78**, 865 (2006)
- [48] T. Maier, M. Jarrell, T. Pruschke, and M.H. Hettler, *Rev. Mod. Phys.* **77**, 1027 (2005)
- [49] G. Moeller, V. Dobrosavljević, and A.E. Ruckenstein, *Phys. Rev. B* **59**, 6846 (1999)
- [50] M. Civelli *et al.*, *Phys. Rev. Lett.* **95**, 106402 (2005)
- [51] G. Lantz *et al.*, *Nat. Commun.* **8**, 13917 (2017)
- [52] V.R. Morrison *et al.*, *Science* **346**, 445 (2014)
- [53] R. Yoshida *et al.*, *Phys. Rev. B* **89**, 205114 (2014)
- [54] O. Nájera: *Study of the dimer Hubbard Model within Dynamical Mean Field Theory and its application to VO₂* (Ph.D. Thesis Université Paris-Saclay 2017) <https://tel.archives-ouvertes.fr/tel-01690699>
- [55] J.K. Freericks, V.M. Turkowski, and V. Zlatić, *Phys. Rev. Lett.* **97**, 266408 (2006)
- [56] D. Silver *et al.*, *Nature* **529**, 484 (2016)
- [57] P.A. Merolla *et al.*, *Science* **345**, 668 (2014)
- [58] US Patent 15307269: *Single-component artificial neuron based on Mott insulators, network of artificial neurons and corresponding manufacturing method*, Inventors: L. Cario, B. Corraze, P. Stoliar, V. Tranchant, E. Janod, M.-P. Belsand, and M.J. Rozenberg
- [59] D.W. Gerstner, W.M. Kistler, R. Naud, and L. Paninski: *Neuronal Dynamics: From Single Neurons to Networks and Models of Cognition* (Cambridge University Press, 2014)
- [60] A. Camjayi *et al.*, *Phys. Rev. Lett.* **113**, 086404 (2014)
- [61] P. Stoliar *et al.*, *Adv. Mater.* **25**, 3222 (2013)
- [62] M.D. Pickett *et al.*, *Nat. Mater.* **12**, 114 (2013)